

Received: 2018.01.11
Accepted: 2018.03.05
Published: 2018.03.21

Measurement of Serum and Hepatic Eicosanoids by Liquid Chromatography Tandem-Mass Spectrometry (LC-MS/MS) in a Mouse Model of Hepatocellular Carcinoma (HCC) with Delivery of c-Met and Activated β -Catenin by Hepatocyte Hydrodynamic Injection

Authors' Contribution:
Study Design A
Data Collection B
Statistical Analysis C
Data Interpretation D
Manuscript Preparation E
Literature Search F
Funds Collection G

ABCD 1 **Yanjie Li***
BF 1 **Nan Lin***
CG 1 **Jianliang Xu**
CG 1 **Yi Lu**
DF 1 **Shuxian Chen**
DG 1 **Chuzhi Pan**
AD 1 **Chusi Wang**
CG 1 **Mingxing Xu**
DG 1 **Boxuan Zhou**
AG 1 **Ruiyun Xu**
AE 2 **Yong-Jiang Xu**

1 Department of Hepatobiliary Surgery, The Third Affiliated Hospital of Sun Yat-sen University, Guangzhou, Guangdong, P.R. China
2 School of Food Science and Technology, Jiangnan University, Wuxi, Jiangsu, P.R. China

* Contributed equally

Corresponding Authors:

Ruiyun Xu, e-mail: xuruiyun@mail.sysu.edu.cn, Yong-Jiang Xu, e-mail: yjxutju@gmail.com

Source of support:

This work was supported by grants from National Natural Science Foundation of China (No. 81760112), Science and Technology Planning Project of Guangdong Province (No. 2016A020212004) and project funding from the China Postdoctoral Science Foundation (No. 2016m602910)

Background: Most forms of cancer, including hepatocellular carcinoma (HCC), are associated with varying degrees of chronic inflammation. The association between the expression of eicosanoids, which are bioactive lipid mediators of inflammation, and HCC remains unknown. The aim of this study was to measure serum and hepatic eicosanoids in a mouse model of HCC with the delivery of c-Met and activated β -catenin by hepatocyte hydrodynamic injection.

Material/Methods: The HCC mouse model, and normal control mice, were used in this study with co-delivery of human c-Met combined with activated β -catenin into hepatocytes through hydrodynamic injection. Liquid chromatography tandem-mass spectrometry (LC-MS/MS) analysis was used to measure serum and hepatic eicosanoid levels.

Results: The combined activation of c-Met and β -catenin was induced in the HCC mouse model. LC-MS/MS showed that a total of 13 eicosanoids in serum and 12 eicosanoids in liver tissue were significantly increased in the HCC mice, when compared with control mice.

Conclusions: In a mouse model of HCC, co-activation of the c-Met and β -catenin signaling pathway resulted in increased levels of serum and hepatic eicosanoids.

MeSH Keywords: **Carcinoma, Hepatocellular • Eicosanoids • Inflammation**

Full-text PDF: <https://www.medscimonit.com/abstract/index/idArt/908931>

 3579

 1

 4

 51



Background

Worldwide, hepatocellular carcinoma (HCC) is the third leading cause of cancer-related death and has become a major global health issue [1]. Previously published epidemiological studies have shown that up to 80% of cases of HCC in humans develop in fibrotic or cirrhotic livers as a consequence of chronic liver injury [2]. The chronic inflammatory response in the liver may have a role in the promotion of HCC increasing hepatocyte cell proliferation and preventing apoptosis [3]. Although some molecular markers have been identified to have prognosis potential in HCC [4–6], specific diagnostic biomarkers for HCC remain to be determined [7].

Eicosanoids are derived from omega-6 or omega-3 fatty acids, particularly arachidonic acid (AA) and linoleic acid (LA). There are multiple subfamilies of eicosanoids, including prostaglandins (PGs) and thromboxane, formed by cyclooxygenase (COX); leukotrienes (LTs) and lipoxins (LXs), formed by lipoxygenases (LOX); and epoxyeicosatrienoic acids (EETs), formed by cytochrome P450 enzymes [8]. Epidemiological, clinical, and pre-clinical animal studies have provided evidence that activation of COX and LOX pathways result in the aberrant metabolism of eicosanoids, and have been involved in multiple pathological processes including inflammation and cancer [9–11]. At this time, few studies have examined the role of eicosanoids in the pathogenesis or progression of HCC [12].

The protein, c-Met, which is also called tyrosine-protein kinase Met, or receptor for hepatocyte growth factor (HGF) is encoded by the *MET* proto-oncogene; β -catenin is a protein that is encoded by the *CTNNB1* gene in humans. The c-Met protein can be stimulated when binding to HGF and activates mitogen-activated protein kinase (MAPK) signaling through the Ras/Raf/MEK/ERK signaling pathway [13,14]. Overexpression of the *MEK* gene has been shown in between 20-50% of patients with HCC [15]. Also, β -catenin is the major downstream effector of the Wnt/ β -catenin signaling pathway, and Wnt signals will suppress the β -catenin protein from degradation, which will result in β -catenin localizing to the cell nucleus with nuclear transcriptional factors triggering downstream gene expression [16,17]. Approximately 30% patients with HCC have *CTNNB1* gene mutations [18]. In humans, oncogenesis in HCC is recognized to be a multistep process involving multiple molecular events and no one single gene mutation results in tumor formation.

The new technique of hydrodynamic transfection involves cell injection with the Sleeping Beauty (SB) transposon system, which can integrate foreign sequences of DNA in the genome of mouse somatic cells, resulting in long-term expression *in vivo*. Therefore, transposition-mediated somatic integration of a specific oncogene can now be used to generate tumors of

defined genetic origin [19,20]. Liu et al. [21], from the University of Pittsburgh, first applied this technique to delivery exogenous gene into hepatocytes. Co-delivery of human c-Met, combined with a constitutively active version of β -catenin, into mouse hepatocyte can successfully induce HCC in two months following injection [19,20]. This technique offers a novel way to develop an animal model of HCC.

In this study, we sought to reveal the role of eicosanoids in the pathogenesis and progression of HCC. We hypothesized that serum and hepatic eicosanoids are altered in HCC mice. We developed HCC mice model by co-delivering human c-Met combined with activated β -catenin into hepatocytes through hydrodynamic injection and determined eicosanoid levels in serum and liver tissue. The findings showed several eicosanoids are increased in HCC mice when compared with healthy animals. The result of this study emphasizes that eicosanoids are meaningful biomarkers that involved in hepatocarcinogenesis.

The aim of this study was to measure serum and hepatic eicosanoids using liquid chromatography tandem-mass spectrometry (LC-MS/MS) analysis in a mouse model of hepatocellular carcinoma (HCC) with the delivery of c-Met and activated β -catenin by hepatocyte hydrodynamic injection.

Material and Methods

Chemicals and reagents

Prostaglandin F2-alpha (PGF2- α); 6-keto-prostaglandin F1-alpha (6-keto-PGF1- α); PGA1, PGB2, PGD2, PGE2, 8-isoPGF2- α , 15-deoxy-PGJ2; thromboxane B2 (TXB2); leukotriene B4 (LTB4); leukotriene E4 (LTE4); 5-hydroxyeicosatetraenoic acid (5-HETE); 5,6-dihydroxyeicosatrienoic acid (5,6-DHET); 12-HETE; 8-HETE; 9-HETE; 5-oxoeicosatetraenoic acid (5-OxoETE); 15-HETE; 16-HETE; 20-HETE; 11,12-DHET, 14,15-DHET; 8,9-epoxy-5Z,8Z,11Z-eicosatrienoic acid (8,9-EET); 11,12-EET; 14,15-EET; 5-hydroxyeicosapentaenoic acid (5-HEPE); 15-HEPE; 9,10-dihydroxy-9Z-octadecenoic acid (9,10-DiHOME); 12,13-DiHOME; 9,10-epoxyoctadecenoic acid (9,10-EpOME); 12,13-EpOME; 9-hydroxyoctadecadienoic acid (9-HODE); 13-HODE; 1-cyclohexyl-dodecanoic acid urea (CUDA); arachidonic acid (ARA); PGF2- α -d4; TXB2-d4; 12,13-EpOME-d4; AA-d8; 9-HODE-d4; and linoleic acid (LA), were obtained from Cayman Chemical (Waterloo, Australia). Formic acid, hexane, acetonitrile and methanol of high-performance liquid chromatography (HPLC) grade were purchased from Sigma Co. (Santa Cruz, CA, USA).

Plasmid constructs

Plasmids, including pT3-EF1 α -hMet (Met), pT3-EF1 α - Δ N90- β -catenin (Cat) and p-CMV-Sleeping Beauty transposase (SB)

were purchased from Addgene global plasmid repository. The SB plasmid provided a reliable means of long-term expression after plasmid-mediated gene delivery.

Mice and the method of hydrodynamic injection

Male C57BL/6J mice, 6-8 weeks old, were raised in a core animal facility and were divided into an experimental group (N=8) and a control group (N=8). For the experimental group, 20 μ g c-Met, 20 μ g β -catenin, and 1.6 μ g of SB plasmid were diluted in 2 ml of 0.9% NaCl, which was sterile filtered, and hydrodynamically injected into the mouse lateral tail vein over a period of between 5-7 seconds. For the control group, mice were injected only with SB. All mice were sacrificed at 2 months and 3 days after injection. Blood was collected from all mice and was incubated for 1 hour prior to serum collection. Excised liver tissues were rinsed in ice-cold phosphate-buffered saline (PBS) and snap-frozen in liquid nitrogen. Samples were stored at -80°C prior to further analysis.

Immunohistochemical staining

Formalin-fixed, paraffin wax-embedded sections of mouse liver were cut onto glass slides, de-paraffinized in xylene and rehydrated in different concentrations of ethanol. Endogenous peroxidases were quenched in 3% H_2O_2 solution. For antigen retrieval, slides were immersed in 10 mM citrate buffer (pH 6.0) and microwaved for 15 minutes. After being blocked with 5% goat serum for 30 minutes, primary antibodies: rabbit polyclonal c-Met (Cell Signaling, Danvers, MA, USA; 8198) at 1: 50 dilution and mouse monoclonal β -catenin (BD Transduction, San Jose, CA, USA; 610154) at 1: 200 dilution were incubated at room temperature for 2 hours. Signals were detected with a 3,3'-diaminobenzidine (DAB) kit (Vector Labs, Burlingame, CA, USA; SK-4100). Slides were counterstained with Mayer's hematoxylin for 5 minutes and viewed using light microscopy.

Protein extraction and Western blotting

Frozen liver tissue samples were homogenized in RIPA buffer with a proteinase and phosphatase inhibitor cocktail (Roche) on ice. Protein concentrations were determined with the Bio-Rad Protein Assay Kit (Bio-Rad, Hercules, CA, USA). Aliquots of 20 μ g denatured protein samples were separated by 12% sodium dodecyl sulfate-polyacrylamide gel electrophoresis (SDS-PAGE) and then transferred to 0.20 μ M nitrocellulose membranes (Invitrogen). After being blocked with 5% non-fat milk powder, the blots were transferred to a 4°C refrigerator for 1.5 hours. Membranes were incubated with the following primary antibodies: rabbit polyclonal c-Met at 1: 1000, mouse monoclonal β -catenin at 1: 2000 and rabbit polyclonal GAPDH at 1: 2000 (Cell Signaling, Danvers, MA, USA; 5174) on shaker at 4°C overnight, followed by incubation with secondary

horseradish peroxidase (HRP)-conjugated antibody (Santa Cruz Biotechnology) diluted 1: 5000 at room temperature, for 2 hours. The blots were developed by the enhanced chemiluminescence (ECL) method (Santa Cruz Biotechnology, Dallas, TX, USA; SC-2048).

Total RNA extraction and quantitative real-time polymerase chain reaction (qRT-PCR)

Total RNA was isolated from frozen liver tissue samples using the TriPure Isolation Reagent (Roche Applied Science, Germany; 11667157001) according to the manufacturer's instructions. Reverse transcription was performed using a Transcriptor First Strand cDNA Synthesis Kit (Invitrogen, Carlsbad, CA, USA; K1612). RT-qPCR was performed with SYBR Green master mixture (Invitrogen, Carlsbad, CA, USA; 4368702).

The primers for *MET* and *CTNNB1* were designed by crossing exon junction, and the sequences were as follows:

MET forward, 5'-GCGCCGTGATGAATATCGAA-3' and reverse, 5'-CG AGAAACCACAACCTGCAT-3';
CTNNB1 forward, 5'-TCCCCTAATGTCCAGC GTT-3' and reverse, 5'-TTAACCACCACCTGGTCCTC-3'; and
GAPDH forward, 5'-AGAAGGCTGGGCTCATTG-3' and reverse, 5'-AGGGGCCATCCACAGTCT TC-3'.

Liquid chromatography tandem-mass spectrometry (LC-MS/MS) analysis

Analysis of eicosanoids by liquid chromatography tandem-mass spectrometry (LC-MS/MS) analysis was based on the methods previously described [22]. Briefly, two different types of compounds were used as internal standards. Type I internal standards were added to samples in extraction to mimic the extraction error, including 12,13-EpOME-d4; PGF2- α -d4; 9-HODE-d4; AA-d8 and TXB2-d4. A synthetic acid, 1-cyclohexyl-dodecanoic acid urea (CUDA), was used as a type II internal standard (0.8 mM in methanol) and added at the last step before analysis, with the purpose to account for changes in volume and instrument variability. The collected serum (20 ml) was spiked with 80 ml type I standards solution. After vortexing, the mixture was dehydrated with N_2 and then reconstituted with 50 ml of type II internal standard.

For analysis of the liver tissue, 2 mgm of lyophilized powdered liver tissue was homogenized in 100 μ l of cold methanol, mixed with type I standard using a bead-based homogenizer, the Tissuelyser LT (Qiagen). The supernatant was ultrasonically extracted (15 min, at 4°C) after being vortexed for 3 minutes. The supernatant was dehydrated with N_2 after two rounds of centrifuging at 16,000 rpm, each for 10 minutes at 4°C , and then reconstituted with 50 ml of type II internal standard.

An Agilent 1200 high-performance liquid chromatography (HPLC) system, equipped with a 6495 triple quadrupole mass detector (Waldbronn, Germany) was loaded with 10 ml of the reconstituted samples. Waters Acquity BEH RPC18 (2.1×100 mm, 1.7 μ m) was used as the column for the separation, and 50°C was set for the oven temperature. The gradient elution used a mobile phase which consisted of (A) acetonitrile/water/acetic acid (60/40/0.02, v/v), and (B) acetonitrile/isopropyl alcohol (50/50, v/v). Then, 0.1% of solution B was used for the initial condition, and a solvent gradient was used as follows: 0-4.0 min, 0.1-55% B; 4.0-4.5 min, 55-99% B; 4.5-5.0 min, 99% B, and using 0.5 mL/min for the flow rate. A negative ion mode was chosen in electrospray ionization mass spectrometry (ESI-MS) for sample analysis. A 3,000 V voltage was used in the ion spray, and 350°C was set for the heated capillary temperature. The nebulizer nitrogen gas and drying gas flow rates were 30 psi and 10 L/min, respectively. A scheduled multiple reaction monitoring (MRM) was used for eicosanoid analysis. Table 1 showed the optimized MRM parameters for the eicosanoids.

Statistical analysis

Data on eicosanoid levels were first presented in a heat map and evaluated by using a non-parametric test, Mann-Whitney, Wilcoxon's test, and Multi-Experiment View V4.6.1 (www.tm4.org). The multivariate statistical analysis was performed by using SIMCA-P software version 11.0 (Umetrics AB, Umea, Sweden). The difference between the results from the experimental and control group was analyzed by visualization of score plots via Orthogonal Projections to Latent Structures Discriminant Analysis (OPLS-DA). The R^2Y value describes the replicability of the data in the set via OPLS-DA analysis. The R^2Y value ranged between 0 and 1, while 1 indicated that the model was replicable. A statistical model with $Q^2 \geq 0.5$ was assumed to have strong predictive power. The false discovery rate (FDR) method of Benjamini and Yekutieli (2001) was used to correct for multiple hypothesis testing and reduce false-positives.

Results

Delivery of human c-Met and β -catenin into mice hepatocytes via hydrodynamic injection

To determine whether exogenous genes could be successfully delivered into mouse liver hepatocytes *in vivo*, the stability of expression of human c-Met (pT3-EF1 α -hMet), activated mutant forms of β -catenin (pT3-EF1 α - Δ N90- β -catenin), along with the sleeping beauty (SB) transposase (p-CMV-Sleeping Beauty transposase) via hydrodynamic injection was evaluated. Western blot experiments showed that protein expressions of exogenous c-Met and Δ N90- β -catenin in the experimental group were significantly increased compared with the control group

(Figure 1A). Also, quantitative real-time polymerase chain reaction (qRT-PCR) analysis demonstrated that mRNA levels of exogenous c-Met and Δ N90- β -catenin were upregulated after gene delivery, but were undetected in the control group (Figure 1B). Immunohistochemical staining also showed the expression of exogenous c-Met in the membrane of hepatocytes in experimental group liver. Both membrane and nuclear β -catenin were detected in sections from liver from the experimental group, whereas only membrane staining was present in sections from the liver of the mice in the control group (Figure 1C).

Overexpression of c-Met and β -catenin triggered liver tumor development in mice

To explore whether overexpression of the c-Met oncogene, *MET*, combined with the activated β -catenin gene, *CTNNB1*, could induce hepatocellular carcinoma (HCC) in mice, plasmids encoding these oncogenes were hydrodynamically injected through the mouse tail vein, while plasmid with only SB transposase was injected in the mouse control group.

Co-expression of c-Met and Δ N90- β -catenin rapidly induced liver tumor formation by eight weeks following injection. There were 6 out of 8 (75%) mice in the experimental group that developed liver tumors, while no tumors were seen in the mouse control group. In the experimental group of mice, the tumors were histologically confirmed to be primary liver tumors, HCC. Macroscopically, these livers were enlarged, and the liver surface showed white tumor nodules (Figure 2A). In the experimental group of six mice who developed HCC, liver weight and the liver/body weight ratio were significantly increased compared with control group (Figure 2C). Due to the lethal tumor burden, the lifespan of the six mice with HCC was significantly reduced compared with the control group (Figure 2D). To confirm that the tumor was induced by exogenous oncogenes, immunohistochemistry for c-Met and β -catenin protein expression were performed. Sections of mouse HCC showed strong positive staining for c-Met and β -catenin, which supported an origin of the tumors from transfected mouse hepatocytes (Figure 2B). These results demonstrated that by using a hydrodynamic transfection technique, a mouse liver cancer model could be induced by the oncogenes of c-Met combined with activated β -catenin.

Multivariate analysis of the eicosanoids profile in mice with HCC

The eicosanoid profile in serum and liver samples from the experimental group of mice with HCC (N=6), and healthy mice (N=8), was investigated using an approach based on mass spectrometry. A total of 36 eicosanoids, representing three metabolic pathways, were screened by liquid chromatography tandem-mass spectrometry (LC-MS/MS) analysis.

Table 1. Scheduled multiple reaction monitoring (MRM) for eicosanoid analysis transitions, collision energy, linear regression equation, linear range, accuracy, and precision of the method.

	Retention time (min)	MRM transition	Collision energy (eV)	Linear regression equation	Correlation coefficient (R ²)	Linear range (nM)	Accuracy (%)	Precision RSD (%)
6-ketePGF1 α	0.76	369->245	-34	y=0.6493x-0.0095	0.995	0.8-2000	89.2	22.6
PGA1	1.77	335->317	-10	y=0.7617x-0.0068	0.996	0.5-1000	91.7	18.2
PGB2	1.61	333->271	-10	y=1.2434x-0.0189	0.994	0.8-2000	88.9	20.1
PGD2	1.45	351->271	-23	y=0.4650x-0.0036	0.999	0.8-2000	90.5	11.7
PGE2	1.27	351->271	-23	y=0.2956x-0.0020	0.997	0.8-1000	92.2	16.0
PGF2 α	1.12	353->193	-35	y=0.4512x-0.0044	0.993	0.8-1000	90.0	15.2
8-isoPGF2 α	0.96	353->193	-33	y=1.5310x-0.0103	0.991	0.4-1000	89.2	17.2
15-deoxy-PGJ2	1.02	315->271	-10	y = 0.008x - 0.582	0.990	0.4-1000	89.9	19.2
TXB2	0.98	369->169	-22	y=1.8027x-0.0136	0.997	0.2-1000	93.4	12.2
LTB4	2.82	335->195	-23	y=0.0605x-5.4701e-4	0.991	20-1000	90.7	21.2
LTE4	2.18	438->333	-33	y=0.3541x-0.0020	0.992	2-1000	90.9	17.9
5-HETE	4.16	319->115	-20	y=0.4201x-0.0037	0.999	1-1000	93.3	11.7
8-HETE	4.05	319->155	-19	y=0.9636x-0.0136	0.995	0.5-2000	95.5	14.3
9-HETE	4.09	319->123	-20	y=0.6061x-0.0032	0.994	0.8-1000	96.4	13.2
12-HETE	4.03	319->135	-19	y=0.1698x-0.0022	0.998	1-2000	92.7	16.8
15-HETE	3.91	319->175	-19	y=0.2228x-0.0021	0.998	4-1000	91.5	15.2
16-HETE	4.02	319->319	-5	y=0.4207x-0.0031	0.991	0.8-1000	92.6	22.3
20-HETE	3.64	319->245	-24	y=0.1074x-6.7859e-4	0.992	0.4-1000	87.8	23.2
5-OxoETE	4.30	317->203	-22	y=0.4093x-8.137e-4	0.990	0.2-1000	86.3	24.8
5,6-DHET	3.65	337->319	-25	y=0.0873x-0.0011	0.993	0.8-1000	87.9	21.0
11,12-DHET	3.33	337->167	-25	y=0.2762x-0.0028	0.992	0.8-1000	88.1	19.1
14,15-DHET	3.19	337->207	-24	y=0.2321x-0.0024	0.991	1-1000	82.9	15.7
8,9-EET	4.38	319->155	-17	y=0.2205x-0.0036	0.993	2-1000	86.3	17.9
11,12-EET	4.34	319->167	-18	y=0.4390x-0.0047	0.993	2-1000	90.2	10.5
14,15-EET	4.23	319->175	-17	y=0.0147x-0.0201	0.996	1-1000	91.6	10.8
5-HEPE	3.77	317->115	-22	y=0.1672x-0.0178	0.997	1-1000	94.4	16.4
15-HEPE	3.61	317->219	-18	y=0.3221x-0.0048	0.998	0.8-1000	92.3	17.4
9,10-DiHOME	3.09	313->201	-29	y=1.6245x-0.0033	0.999	0.4-1000	89.3	11.6
12,13-DiHOME	3.04	313->183	-29	y= 38.14x - 582.1	0.998	0.2-1000	88.4	11.8
9,10-EpOME	4.25	295->171	-21	y=0.012x - 6.497	0.996	0.8-1000	82.4	17.4
12,13-EpOME	4.23	295->195	-23	y=0.4237x-0.0037	0.997	0.6-1000	88.8	16.6
9-HODE	3.88	295->171	-23	y=0.6122x-0.0212	0.999	1-1000	90.4	10.8
13-HODE	3.89	295->195	-23	y=0.5433x-0.0067	0.996	0.3-1000	93.2	10.5
ARA	4.67	303->259	-25	y=195.1x - 42.94	0.999	200-30000	98.6	9.8
LA	4.55	279->220	-29	y=0.107x - 34.50	0.997	150-20000	97.7	10.1

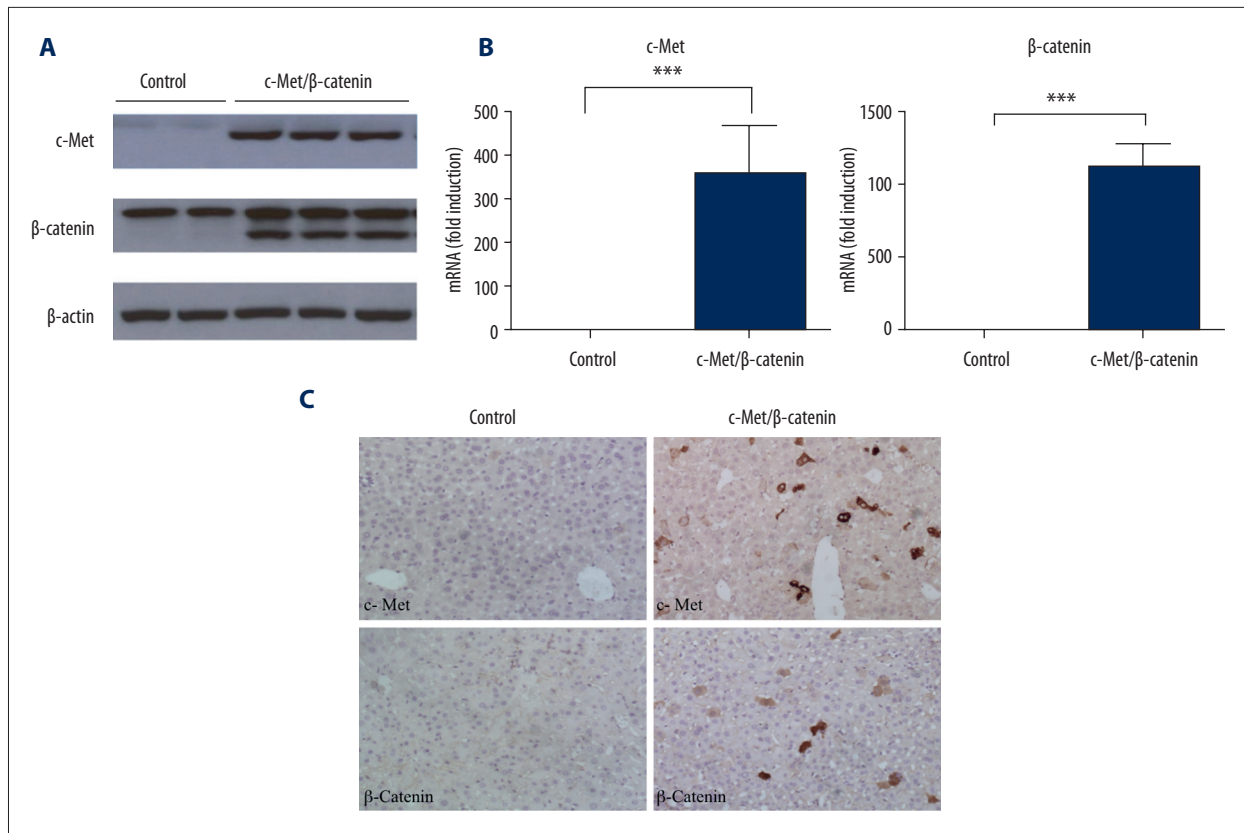


Figure 1. Exogenous c-Met and Δ N90- β -catenin were successfully delivered three days after hydrodynamic injection in mice. **(A)** Protein expression of c-Met and Δ N90- β -catenin in liver lysates three days following hydrodynamic injection into the mice tail veins. **(B)** mRNA level of exogenous c-Met and Δ N90- β -catenin by quantitative real-time polymerase chain reaction (qRT-PCR) analysis. **(C)** Photomicrograph of the immunohistochemistry (brown staining) for c-Met and β -catenin protein expression in mouse liver tissue sections.

A total of 28 and 30 eicosanoids were detected in mouse serum and liver samples respectively. Statistical analysis was performed on these quantified eicosanoids. The serum profile of the experimental HCC mice compared with the control mice showed clear separation by using Orthogonal Projections to Latent Structures Discriminant Analysis (OPLS-DA) plots (Figure 3A). The liver profile also showed similar separation (Figure 3B), with perfect modeling fit R²Y values of 0.938 (serum) and 0.749 (liver), and excellent prediction Q² values of 0.73 (serum) and 0.548 (liver). The first two principal components (PC1 and PC2) explain most of the variation of the metabolites between HCC and the controls, accounting for 35% of the total cumulative variance. A permutation test (N=20) was performed to confirm the reliability of the prediction model (Figure 3C, 3D). The Q²-intercept value was -0.089 (serum) and -0.192 (liver) for the prediction model, which were less than 0.05, indicating that the model was statistically sound, and this result also showed that the high predictability of this model was not because of over-fitting of the data.

Altered eicosanoids in HCC in the experimental group of mice

The LC-MS/MS method for quantification of eicosanoids in mouse serum and liver was validated with standard curve and limit of detection (LOD) (Table 1). The eicosanoid profile was changed in the experimental group of mice with HCC compared with control group. A heat map was performed to describe fold changes for each group (Figure 4A). When compared with the control group, there was a significant change in eicosanoids in the experimental group of mice with HCC, which are shown in the box plots in Figure 4B. Levels of 6-keto-PGF1- α , PGF2- α , PGD2, PGE2, TXB2, LTE4, 5-HETE, 15-HETE, 9,10-DiHOME, 9,10-EpOME, 12,13-EpOME, 5,6-EET and 8,9-EET in serum samples and products of arachidonic acid metabolism were significantly increased in the experimental group of mice with HCC. Also, alterations in 6-keto-PGF1- α , PGF2- α , PGE2, TXB2, 5-HETE, 15-HETE, 5-HEPE, 15-HEPE, 9,10-DiHOME and 12,13-DiHOME in liver samples were also increased in the experimental group of mice with HCC. The linoleic acid metabolite,

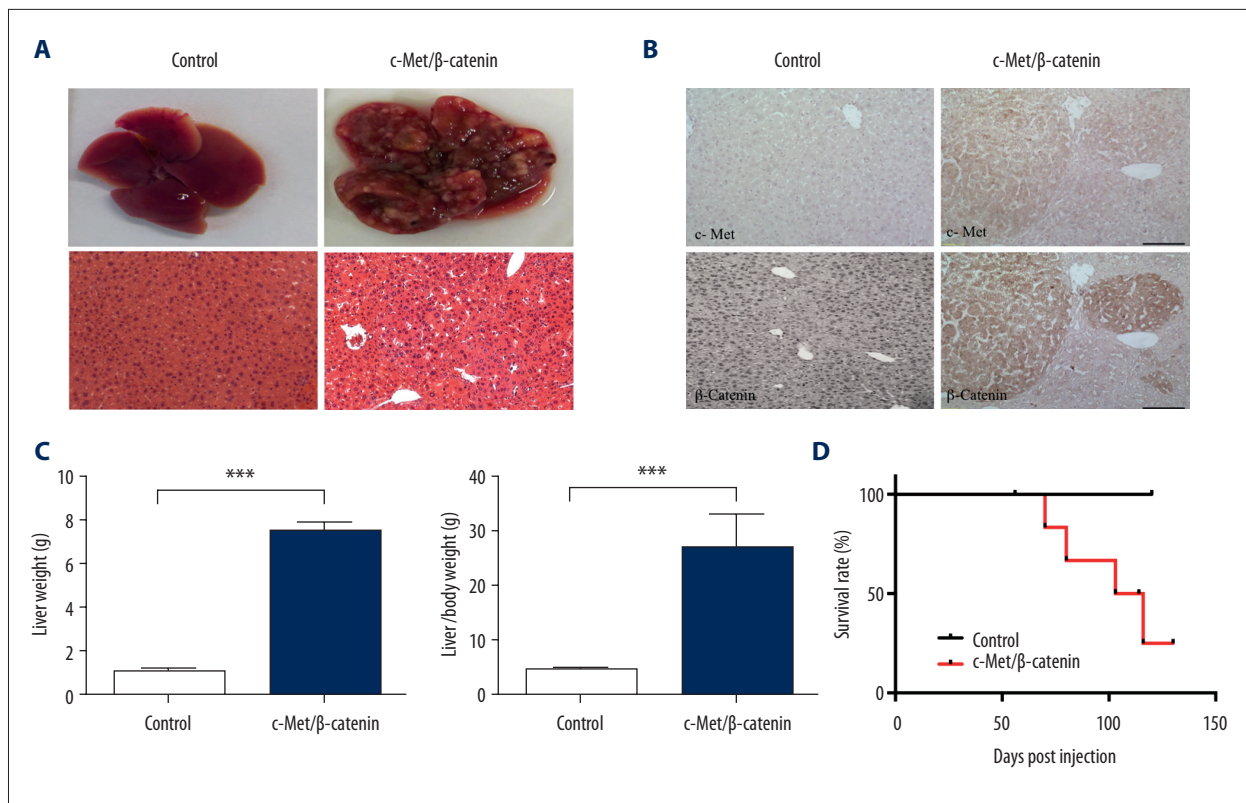


Figure 2. Co-activation of c-Met and Δ N90- β -catenin resulted in liver tumor development in mice. (A) Gross images and hematoxylin staining of tissue sections of mice livers at eight weeks post-injection. (B) Photomicrographs of liver sections were examined by light microscopy following immunohistochemistry with antibody staining for c-Met and β -catenin protein. (C) Liver weight and liver/body weight ratio were compared at eight weeks post-injection. (D) Survival curve following hydrodynamic transfection in mice.

9-HODE, and 13-HODE were also significantly increased in the livers of the experimental group of mice with HCC.

Discussion

Chronic inflammation has a role in the development of hepatocellular carcinoma (HCC) in humans, but the underlying mechanisms remain unclear [23]. Eicosanoids are produced from arachidic acid in the hepatocyte, and when secreted into the blood they act as signaling molecules. Eicosanoids represent a large family of bioactive signaling molecules with diverse and potent biological effects [24–26]. Recent studies have analyzed the levels of eicosanoids in plasma, urine, or tissue from patients with cancer, and have shown that the eicosanoid profiles might have potential as cancer-related biomarkers [27]. Studies on the possible relationships between eicosanoids and HCC may provide unique biological insights into the role of eicosanoids and their modifications in the pathogenesis and progression of HCC. The hepatocyte growth factor (HGF)/c-Met and Wnt/ β -catenin signaling pathways have previously been shown to be dysregulated in human HCC [16,17]. For this reason, the aim

of this study was to co-express the oncogene of c-Met (*MET*) combined with the β -catenin gene (*CTNNB1*) to induce HCC development in mice in an established mouse model.

While the underlying molecular mechanism by which *MET/CTNNB1* induces HCC remains unknown, there is accumulating evidence that c-Met and β -catenin are involved in inflammation during carcinogenesis. A recent study showed that c-Met increases the proliferation activity of endometrial cancer cell through upregulation of COX-2 expression [28]. Also, β -catenin has been reported to trigger an inflammatory response during HCC development in mice through activation of the NF- κ B pathway [29].

In this study, the eicosanoid levels in serum and liver tissue derived from HCC mice were analyzed by a developed approach based on liquid chromatography tandem-mass spectrometry (LC-MS/MS) analysis. The findings showed that serum eicosanoids (6-keto-PGF1- α , PGF2- α , PGD2, PGE2, TXB2, LTE4, 5-HETE, 15-HETE, 9,10-DiHOME, 9,10-EpOME, 12,13-EpOME, 5,6-EET and 8,9-EET) and liver eicosanoids (6-Keto-PGF1- α , PGF2- α , PGE2, TXB2, 5-HETE, 15-HETE, 5-HEPE, 15-HEPE, 9,10-DiHOME,

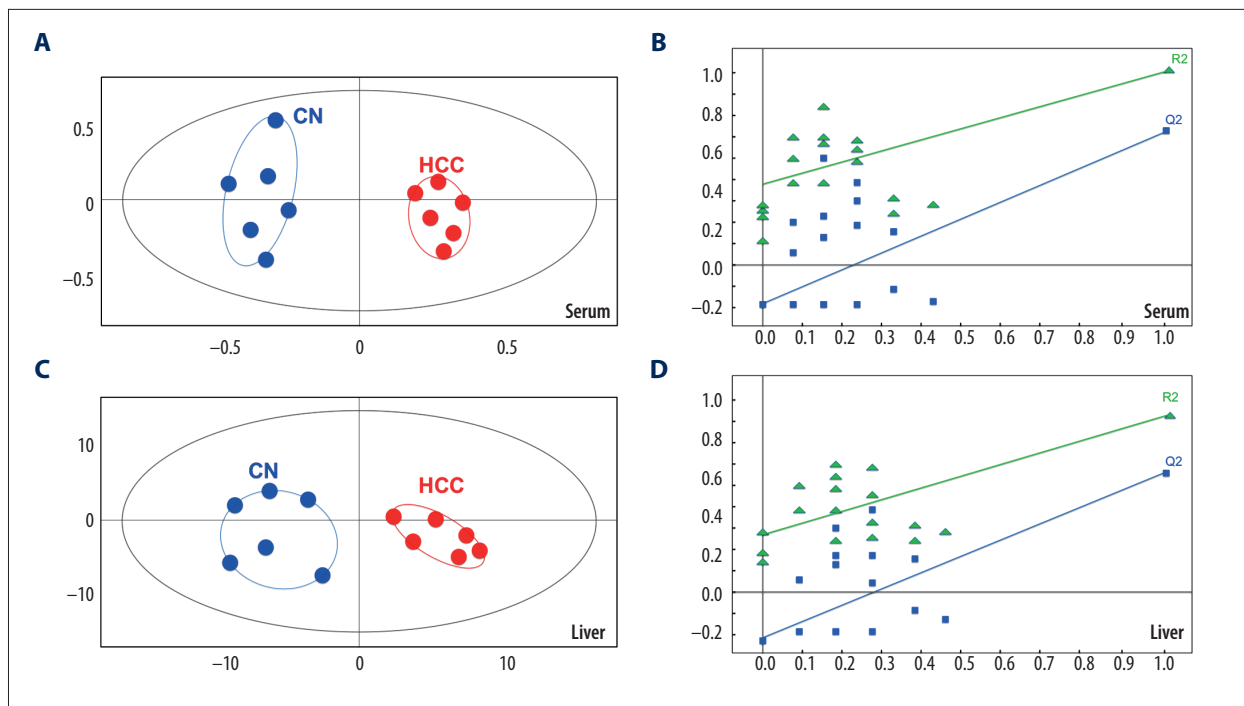


Figure 3. Statistical analysis to compare the control group of mice (CN), with the experimental group of mice with c-Met and β -catenin hepatocellular carcinoma (HCC). **(A, B)** Orthogonal Projections to Latent Structures Discriminant Analysis (OPLS-DA) score plots and validation plots obtained from permutation test ($n=20$) for serum samples. **(C, D)** OPLS-DA score plots and validation plots obtained from permutation test ($n=20$) for liver tissue samples.

12,13-DiHOME, 9-HODE and 13-HODE) were increased in the experimental mouse group with HCC, when compared with controls (Figure 4). The changes in eicosanoids detected in the serum and livers of mice with HCC were consistent with previous studies in other cancer types [12].

Previously published studies have demonstrated that COX-derived prostaglandins and thromboxanes play important roles in carcinogenesis [30–32]. The present study findings showed increased levels of 6-keto-PGF1- α , PGF2- α and PGE2 in both serum and liver tissue from HCC mice. The 6-keto-PGF1- α is a non-enzymatic hydrolysis product of PGI2 and could be used as a marker of PGI2 biosynthesis *in vivo*. Previous studies have shown that the activation of the mTOR/I κ B- α /NF- κ B pathway contributed to increased levels of 6-keto-PGF1- α , which were associated with cell proliferation in human gastric cancer cells [33,34]. Also, PGE2 overexpression has been detected in various solid tumors, including colon, lung, breast, and head and neck cancer, and are associated with a poor prognosis [35–38]. Also, previously published studies have shown that PGE2 treatment increased both small and large intestinal adenoma burden in the ApcMin/+ mouse model of colon cancer and significantly enhanced azoxymethane (AOM)-induced colon tumor incidence and multiplicity [39]. In contrast, the inhibition of endogenous PGE through the genetic deletion of prostaglandin E synthase (PTGES) has been shown to suppress intestinal

tumorigenesis in mouse models [40]. Similarly, PGF2- α , which is a metabolite of PGE2 has also been reported to be increased in several types of carcinoma [41–43]. As shown in a previously published study on non-small cell lung cancer (NSCLC) increased concentrations of TXB2 were also found in mice [44]. It has previously been proposed that thromboxane synthase (TXS) metabolizes prostaglandin H2 into TXB2, which could promote tumor growth through increased tumor angiogenesis [45]. Therefore, it is possible that COX produces prostaglandins and thromboxanes to mediate cell proliferation in HCC.

Few downstream products of the LOX pathway have also been found to be upregulated in mouse models of HCC, and a significant increase in LOX products has been applied to characterize inflammation [46]. 5-HETE has been proposed as an indicator in many disease states where acute or chronic inflammation is part of the pathophysiology of the disease [47]. The findings of the present study support the findings of these previous studies, as the levels of 5-HETE were found to be increased in the experimental group of mice with HCC. Also, levels of 5-HETE have previously been shown to be increased in prostate cancer [48]. In a previous study, overproduction of 15-HETE was observed *in vitro* in the human colon cancer cell line, HCA-7, and in HCA-7 tumors in an animal model [49]. Also, in the present study, 9,10-DiHOME was increased in the experimental group of mice with HCC. The 9,10-DiHOME molecule is

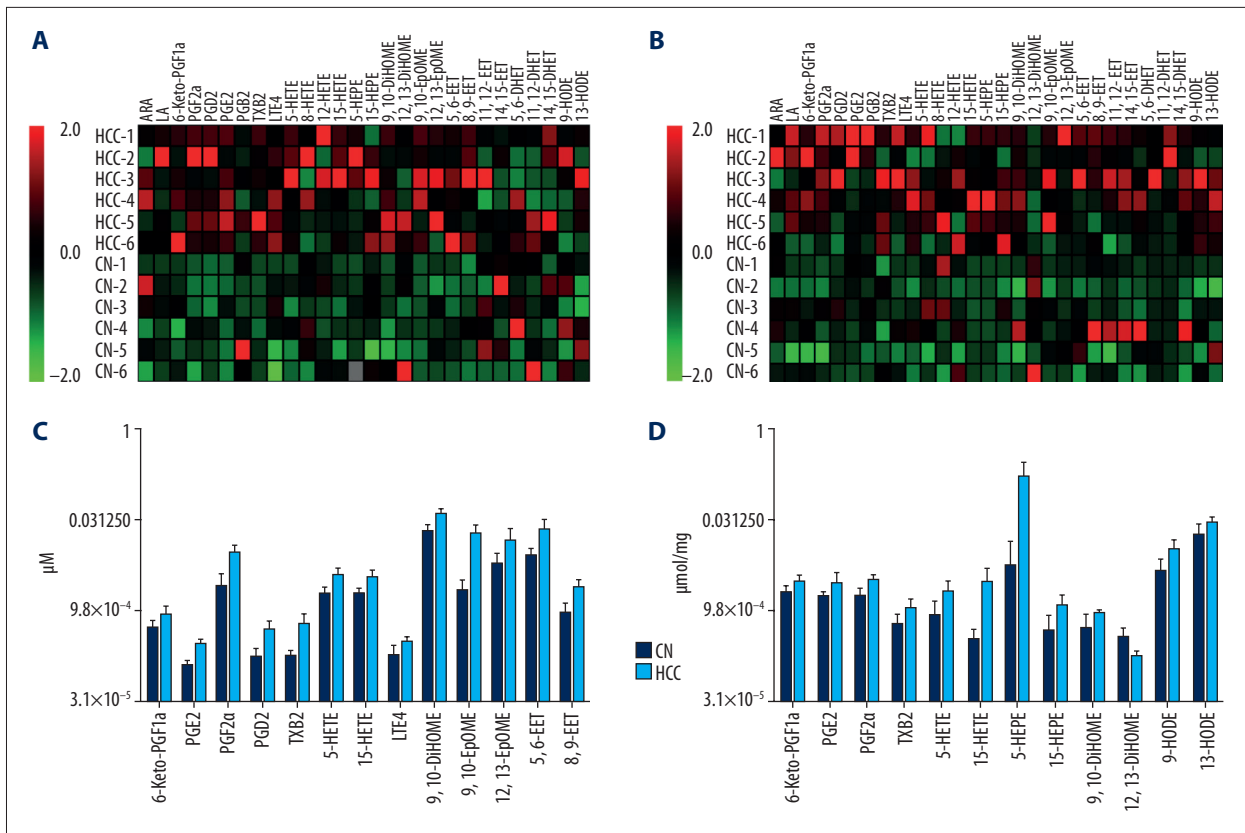


Figure 4. Eicosanoid changes in serum and liver tissue induced by overexpression of C-Met and β -catenin. (A) All detected serum eicosanoid level changes are expressed as a heat map. (B) All detected liver eicosanoid level changes are expressed as a heat map. Fold changes are derived from the fold difference compared with normalized means for each eicosanoid. Green squares indicate a reduction of up to two-fold; black squares indicate no significant fold changes; red squares indicate an increase of up to two-fold. (C) Concentrations of significantly changed eicosanoids detected in mouse serum. (D) Concentrations of significantly changed eicosanoids detected in mouse liver tissue.

an epoxide and diol metabolite of linoleic acid (LA), which has been proposed as a potential diagnostic biomarker in several human diseases [50]. Also, 9,10-DiHOME can be synthesized *de novo* as a result of inflammation and oxidative stress [51]. The findings of these previous studies might explain the finding in the present study of the increase in the concentration of 9,10-DiHOME in serum and liver samples of mice with HCC.

Conclusions

In a mouse model of hepatocellular carcinoma (HCC), co-activation of the c-Met and β -catenin signaling pathways resulted in increased levels of serum and hepatic eicosanoids. The

findings of this study support the value of a mouse model that used the new technique of hydrodynamic transfection, which can integrate foreign DNA sequences in the genome of mouse somatic cells, resulting in long-term expression *in vivo*. Also, the findings of this study have provided new insights into changes in the eicosanoid profile in HCC, and reinforce current knowledge that eicosanoids are biologically relevant molecules involved in cancer progression. Further studies are recommended on the measurement of serum and hepatic eicosanoids as potential biomarkers for HCC.

Conflict of interest.

None.

References:

1. Ghouri YA, Mian I, Rowe JH: Review of hepatocellular carcinoma: Epidemiology, etiology, and carcinogenesis. *J Carcinogens*, 2017; 16: 1
2. Clark T, Maximin S, Meier J et al: Hepatocellular carcinoma: Review of epidemiology, screening, imaging diagnosis, response assessment, and treatment. *Curr Problems Diagn Radiol*, 2015; 44: 479–86
3. Jin K, Li T, Sanchez-Duffhues G et al: Involvement of inflammation and its related microRNAs in hepatocellular carcinoma. *Oncotarget*, 2017; 8: 22145–65
4. Umeda S, Kanda M, Kodera Y: Emerging evidence of molecular biomarkers in hepatocellular carcinoma. *Histol Histopathol*, 2017 [Epub ahead of print]
5. Klingenberg M, Matsuda A, Diederichs S et al: Non-coding RNA in hepatocellular carcinoma: Mechanisms, biomarkers and therapeutic targets. *J Hepatol*, 2017; 67: 603–18
6. Zheng C, Liu X, Chen L et al: lncRNAs as prognostic molecular biomarkers in hepatocellular carcinoma: A systematic review and meta-analysis. *Oncotarget*, 2017; 8: 59638–47
7. Fujiwara N, Friedman SL, Goossens N et al: Risk factors and prevention of hepatocellular carcinoma in the era of precision medicine. *J Hepatol*, 2018; 68(3): 526–49
8. Haeggstrom JZ, Rinaldo-Matthis A, Wheelock CE et al: Advances in eicosanoid research, novel therapeutic implications. *Biocgem Biophys Res Commun*, 2010; 396: 135–39
9. Moore GY, Pidgeon GP: Cross-talk between cancer cells and the tumour microenvironment: The role of the 5-lipoxygenase pathway. *Int J Mol Sci*, 2017; 18(2): pii: E236
10. Echizen K, Hirose O, Maeda Y et al: Inflammation in gastric cancer: Interplay of the COX-2/prostaglandin E2 and Toll-like receptor/MyD88 pathways. *Cancer Sci*, 2016; 107: 391–97
11. Yu T, Lao X, Zheng H: Influencing COX-2 activity by COX related pathways in inflammation and cancer. *Mini Rev Med Chem*, 2016; 16: 1230–43
12. Wang D, Dubois RN: Eicosanoids and cancer. *Nat Rev Cancer*, 2010; 10: 181–93
13. Giordano S, Columbano A: Met as a therapeutic target in HCC: Facts and hopes. *J Hepatol*, 2014; 60: 442–52
14. Trusolino L, Bertotti A, Comoglio PM: MET signalling: Principles and functions in development, organ regeneration and cancer. *Nat Rev Mol Cell Biol*, 2010; 11: 834–48
15. Taviani D, De Petro G, Benetti A et al: u-PA and c-MET mRNA expression is co-ordinately enhanced while hepatocyte growth factor mRNA is down-regulated in human hepatocellular carcinoma. *Int J Cancer*, 2000; 87: 644–49
16. Clevers H: Wnt/ β -catenin signaling in development and disease. *Cell*, 2006; 127: 469–80
17. Kohn AD, Moon RT: Wnt and calcium signaling: β -catenin-independent pathways. *Cell Calcium*, 2005; 38: 439–46
18. de La Coste A, Romagnolo B, Billuart P et al: Somatic mutations of the β -catenin gene are frequent in mouse and human hepatocellular carcinomas. *Proc Natl Acad Sci USA*, 1998; 95: 8847–51
19. Tward AD, Jones KD, Yant S et al: Distinct pathways of genomic progression to benign and malignant tumors of the liver. *Proc Natl Acad Sci USA*, 2007; 104: 14771–76
20. Patil MA, Lee SA, Macias E et al: Role of cyclin D1 as a mediator of c-Met- and β -catenin-induced hepatocarcinogenesis. *Cancer Res*, 2009; 69: 253–61
21. Liu F, Song Y, Liu D: Hydrodynamics-based transfection in animals by systemic administration of plasmid DNA. *Gene Ther*, 1999; 6: 1258–66
22. Xu YJ, Ho WE, Xu F et al: Exploratory investigation reveals parallel alteration of plasma fatty acids and eicosanoids in coronary artery disease patients. *Prostaglandins Other Lipid Mediat*, 2013; 106: 29–36
23. Pinato DJ, Merli M, Dalla Pria A et al: Systemic inflammatory response is a prognostic marker in HIV-infected patients with hepatocellular carcinoma. *Oncology*, 2017; 93: 395–400
24. Jamieson KL, Endo T, Darwesh AM et al: Cytochrome P450-derived eicosanoids and heart function. *Pharmacol Ther*, 2017; 179: 47–83
25. Esser-von Bieren J: Immune-regulation and -functions of eicosanoid lipid mediators. *Biol Chem*, 2017; 398: 1177–91
26. Calder PC: Omega-3 fatty acids and inflammatory processes: from molecules to man. *Biochem Soc Trans*, 2017; 45: 1105–15
27. Piazzuelo E, Lanas A: NSAIDs and gastrointestinal cancer. *Prostaglandins Other Lipid Mediat*, 2015; 120: 91–96
28. Yoshizawa Y, Yamada Y, Kanayama S et al: Signaling pathway involved in cyclooxygenase-2 upregulation by hepatocyte growth factor in endometrial cancer cells. *Oncology Rep*, 2011; 26: 957–64
29. Anson M, Crain-Denoyelle AM, Baud V et al: Oncogenic β -catenin triggers an inflammatory response that determines the aggressiveness of hepatocellular carcinoma in mice. *J Clin Invest*, 2012; 122: 586–99
30. Cui Y, Shu XO, Li HL et al: Prospective study of urinary prostaglandin E2 metabolite and pancreatic cancer risk. *Int J Cancer*, 2017; 141: 2423–29
31. Che D, Zhang S, Jing Z et al: Macrophages induce EMT to promote invasion of lung cancer cells through the IL-6-mediated COX-2/PGE2/ β -catenin signalling pathway. *Molec Immunol*, 2017; 90: 197–210
32. Ye Y, Liu M, Yuan H et al: COX-2 regulates Snail expression in gastric cancer via the Notch1 signaling pathway. *Int J Molec Med*, 2017; 40: 512–22
33. Temiz-Resitoglu M, Kucukkavruk SP, Guden DS et al: Activation of mTOR/IkappaB-alpha/NF-kappaB pathway contributes to LPS-induced hypotension and inflammation in rats. *Eur J Pharmacol*, 2017; 802: 7–19
34. Lim JW, Kim H, Kim KH: Nuclear factor-kappaB regulates cyclooxygenase-2 expression and cell proliferation in human gastric cancer cells. *Lab Invest*, 2001; 81: 349–60
35. Hsu HH, Lin YM, Shen CY et al: Prostaglandin E2-induced COX-2 expressions via EP2 and EP4 signaling pathways in human LoVo colon cancer cells. *Int J Mol Sci*, 2017; 18(6): pii: E1132
36. Bhooshan N, Staats PN, Fulton AM et al: Prostaglandin E receptor EP4 expression, survival and pattern of recurrence in locally advanced NSCLC. *Lung Cancer*, 2016; 101: 88–91
37. Qin W, Holick MF, Sorensen W et al: Vitamin D3 treatment influences PGE2 and TGFbeta in normal and increased breast cancer risk women. *Anticancer Res*, 2016; 36: 5347–53
38. Kumai T, Oikawa K, Aoki N et al: Tumor-derived TGF-beta and prostaglandin E2 attenuate anti-tumor immune responses in head and neck squamous cell carcinoma treated with EGFR inhibitor. *J Transl Med*, 2014; 12: 265
39. Wang D, Wang H, Shi Q et al: Prostaglandin E(2) promotes colorectal adenoma growth via transactivation of the nuclear peroxisome proliferator-activated receptor delta. *Cancer Cell*, 2004; 6: 285–95
40. Nakanishi M, Montrose DC, Clark P et al: Genetic deletion of mPGES-1 suppresses intestinal tumorigenesis. *Cancer Res*, 2008; 68: 3251–59
41. Yoda T, Kikuchi K, Miki Y et al: 11beta-prostaglandin F2alpha, a bioactive metabolite catalyzed by AKR1C3, stimulates prostaglandin F receptor and induces slug expression in breast cancer. *Mol Cell Endocrinol*, 2015; 413: 236–47
42. Gong J, Xie J, Bedolla R et al: Combined targeting of STAT3/NF-kappaB/COX-2/EP4 for effective management of pancreatic cancer. *Clin Cancer Res*, 2014; 20: 1259–73
43. Brys M, Morel A, Forma E et al: Relationship of urinary isoprostanes to prostate cancer occurrence. *Mol Cell Biochem*, 2013; 372: 149–53
44. Huang RY, Li SS, Guo HZ et al: Thromboxane A2 exerts promoting effects on cell proliferation through mediating cyclooxygenase-2 signal in lung adenocarcinoma cells. *J Cancer Res Clin Oncol*, 2014; 140: 375–86
45. Cathcart MC, Gately K, Cummins R et al: Thromboxane synthase expression and correlation with VEGF and angiogenesis in non-small cell lung cancer. *Biochim Biophys Acta*, 2014; 1842: 747–55
46. Kuhn H, Banthiya S, van Leyen K: Mammalian lipoxygenases and their biological relevance. *Biochim Biophys Acta*, 2015; 1851: 308–30
47. Radmark O, Werz O, Steinhilber D et al: 5-Lipoxygenase, a key enzyme for leukotriene biosynthesis in health and disease. *Biochim Biophys Acta*, 2015; 1851: 331–39
48. Rodriguez-Blanco G, Burgers PC, Dekker LJ et al: Serum levels of arachidonic acid metabolites change during prostate cancer progression. *Prostate*, 2014; 74: 618–27
49. Chang J, Jiang L, Wang Y et al: 12/15 Lipoxygenase regulation of colorectal tumorigenesis is determined by the relative tumor levels of its metabolite 12-HETE and 13-HODE in animal models. *Oncotarget*, 2015; 6: 2879–88
50. Zhang Y, Guallar E, Blasco-Colmenares E et al: Serum-based oxylipins are associated with outcomes in primary prevention implantable cardioverter defibrillator patients. *PLoS One*, 2016; 11: e0157035
51. Gouveia-Figueira S, Spath J, Zivkovic AM et al: Profiling the oxylipin and endocannabinoid metabolome by UPLC-ESI-MS/MS in human plasma to monitor postprandial inflammation. *PLoS One*, 2015; 10(7): e0132042